Journal of Power Sources 184 (2008) 392–401

Contents lists available at ScienceDirect

Journal of Power Sources

journal homepage: www.elsevier.com/locate/jpowsour

Electrochemical performance of $LiCoO_2$ cathodes by surface modification using lanthanum aluminum garnet

Cheng-Zhang Lu[a], Jin-Ming Chen[b], Yung-Da Cho[a], Wen-Hsiang Hsu[a], P. Muralidharan[a], George Ting-Kuo Fey[a,*]

[a] Department of Chemical and Materials Engineering, National Central University, Chung-Li 320, Taiwan
[b] Material Chemical Laboratories, Industrial Technology Research Institute, Hsinchu 310, Taiwan

ARTICLE INFO

Article history:
Received 15 January 2008
Received in revised form 15 April 2008
Accepted 24 April 2008
Available online 13 May 2008

Keywords:
Cathodes
Coating
$3LaAlO_3$:Al_2O_3
$LiCoO_2$
Lithium-ion battery

ABSTRACT

$LiCoO_2$ particles were coated with various wt.% of lanthanum aluminum garnets ($3LaAlO_3$:Al_2O_3) by an in situ sol–gel process, followed by calcination at 1123 K for 12 h in air. X-ray diffraction (XRD) patterns confirmed the formation of a $3LaAlO_3$:Al_2O_3 compound and the in situ sol–gel process synthesized $3LaAlO_3$:Al_2O_3-coated $LiCoO_2$ was a single-phase hexagonal α-$NaFeO_2$-type structure of the core material without any modification. Scanning electron microscope (SEM) images revealed a modification of the surface of the cathode particles. Transmission electron microscope (TEM) images exposed that the surface of the core material was coated with a uniform compact layer of $3LaAlO_3$:Al_2O_3, which had an average thickness of 40 nm. Galvanostatic cycling studies demonstrated that the 1.0 wt.% $3LaAlO_3$:Al_2O_3-coated $LiCoO_2$ cathode showed excellent cycle stability of 182 cycles, which was much higher than the 38 cycles sustained by the pristine $LiCoO_2$ cathode material when it was charged at 4.4 V.

1. Introduction

The most popular cathode material used in commercial lithium-ion batteries is $LiCoO_2$ because of its high electronic conductivity, good rate capability, ease of preparation and excellent cycling performance with a stable layered structure, where Li^+ and Co^{3+} ions occupy alternate (1 1 1) planes of a rock salt structure [1–5]. The $LiCoO_2$ cathode material exhibits excellent electrochemical performance with a high theoretical capacity of 274 mAh g^{-1} [6]. However, from the layered structure, only 0.5 mol of lithium ion is extractable within the voltage range of 3–4.2 V vs. Li^+/Li, which can deliver a reversible capacity of around 140 mAh g^{-1} of the theoretical capacity of $LiCoO_2$ [7]. Alternatively, a higher capacity could be obtained from this material by charging it beyond 4.2 V vs. Li^+/Li, which generally leads to a dissolution of strongly oxidized Co^{4+} ions into the electrolyte and a fast impedance growth on the surface of the cathode during the (de)lithiation process, thereby negatively affecting capacity retention (C.R.) and cycle stability [8,9].

In order to prevent major chemical side reactions on the surface of the cathode materials, novel approaches have been developed to coat the surface of cathode materials with various oxides to improve electrode performance in terms of cyclability, thermal stability, and high temperature capacity. Various groups of researchers have followed the surface coating technique to coat both layered and spinel cathode oxides, which resulted in improved cycle stability and capacity retention even at higher voltages of the lithium extraction process. The surface of the cathode materials coated with $Li_2O{\cdot}2B_2O_3$ [10], $Li_4Ti_5O_{12}$ [11], La_2O_3 [12], $ZrTiO_4$ [13], Al_2O_3 [8,14–16], ZrO_2 [7,8,14,17], CeO_2 [18], metal phosphate [19–21] and $MgAl_2O_4$ [22] demonstrated enhanced cycling performance in terms of higher capacity. The materials used for surface coating play a significant role by shielding the highly active core material, thereby preventing many side reactions that would lead to faster impedance growth. Chung et al. [17] have reported using in situ X-ray diffraction (XRD) to study the effect of a ZrO_2 coating buffer layer on capacity retention during high voltage cycling when the cathode was protected from the electrolyte.

The surface coating procedure and the materials [7,8,10–21] employed for coating are integral to the configuration of a uniform and well-adhered coating on the surface of the core material with low temperature syntheses. In general, ceramic materials are suitable candidates due to their high thermo-mechanical stability, resistance to both oxidizing and reducing atmospheres at high temperatures, and resistance to attack by moisture and chemical

* Corresponding author. Tel.: +886 3 425 7325; fax: +886 3 425 7325.
E-mail address: gfey@cc.ncu.edu.tw (G.T.-K. Fey).

0378-7753/$ – see front matter © 2008 Elsevier B.V. All rights reserved.
doi:10.1016/j.jpowsour.2008.04.087

reactions. Among the ceramic materials currently being investigated, yttrium aluminum garnet (YAG) and lanthanum aluminum garnet (LAG) ceramic powders are promising materials for optical, electronic and structural applications [23–25]. In particular, lanthanum aluminum garnet mainly formed as $3LaAlO_3{:}Al_2O_3$ instead of single $La_3Al_5O_{12}$, with alumina that are possibly amorphous [23], finds many applications as superconducting devices and dielectric materials with good thermal stability. The $3LaAlO_3{:}Al_2O_3$ coating may play a dual role in improving electrochemical properties of coated cathodes. Amorphous alumina acts as an amphoteric oxide that scavenges PF_6^- anion and its related contaminants (HF and PF_5) produced during the cycling process in the liquid electrolyte. $LaAlO_3$ forms an adherent coating surface on the cathode material and acts as an electronic conductor under specific circumstances [26–28]. In this paper, we have attempted to synthesize different wt.% $3LaAlO_3{:}Al_2O_3$-coated $LiCoO_2$ cathode materials by an in situ sol–gel process and study their electrochemical performance at higher charging voltages.

2. Experimental

2.1. Synthesis of lanthanum aluminum garnet by a sol–gel process

Lanthanum aluminum garnet ceramic powders were synthesized by an alkoxide sol–gel process [23]. Analytical grade chemicals of lanthanum nitrate hexahydrate ($La(NO_3)_3{\cdot}6H_2O$, Aldrich), aluminum nitrate nonahydrate ($Al(NO)_3{\cdot}9H_2O$, Aldrich) and ethylene glycol (EG) were used in the preparation process. Initially, $Al(NO)_3{\cdot}9H_2O$ and $La(NO_3)_3{\cdot}6H_2O$ were dissolved separately in deionized water with continuous stirring. Ethylene glycol was added as a complexing agent and mixed together to form the lanthanum alumina sol precursor solution. The sol was allowed to set into a gel at 343 K, maintained in an oven and later the gel was aged at 393 K for 48 h. The dried gel was heated at 1023 and 1273 K for 10 h at a heating ramp of 2 K min^{-1} to yield crystalline $3LaAlO_3{:}Al_2O_3$ ceramic powders.

2.2. In situ sol–gel synthesis of lanthanum aluminum garnet coated $LiCoO_2$

Fig. 1 represents the in situ sol–gel coating procedure for the synthesis of $3LaAlO_3{:}Al_2O_3$-coated $LiCoO_2$ cathode material. The calculated amount of $LiCoO_2$ cathode powders was dispersed in deionized water and sonicated for 5 h and then added to the in situ synthesized $3LaAlO_3{:}Al_2O_3$ sol precursor under sonication for 0.5 h. The sonicated mixture was continuously stirred for 10 h at 353 K. The excess EG and water were evaporated to form a thick black gel. The gel was dried in an oven at 393 K for 48 h to form a dry black powder, which was calcined at 1023, 1123 and 1223 K for 12 h in air at a heating ramp of 2 K min^{-1} to form a thin buffer layer of $3LaAlO_3{:}Al_2O_3$ coating on $LiCoO_2$ within the weight ratios of 0.5:99.5, 1.0:99.0 and 1.5:98.5, respectively.

Structural and phase analyses were carried out using a powder X-ray diffractometer, Siemens D-5000, Mac Science MXP18, equipped with a nickel-filtered Cu Kα radiation source (λ = 1.5405 Å). The diffraction patterns were recorded between scattering angles of 15° and 80° in steps of 0.05°. The surface morphology of the coated materials was studied using a scanning electron microscope, Hitachi model S-3500V. The sol–gel synthesized $3LaAlO_3{:}Al_2O_3$ particle size and the coating layer morphology of the coated particles were examined by a JEOL JEM-200FXII transmission electron microscope (TEM) equipped with a LaB_6 gun. The sample for transmission electron microscope study was prepared by dispersing the powder in ethanol, placing a drop of the clear solution on a carbon-coated copper grid, and subsequent drying. X-ray photon spectroscopy (XPS) and the depth profiles were recorded by an electron spectroscopy for chemical analysis (ESCA) instrument (VG Scientific ESCALAB 250) with monochromatic Al Kα radiation 1486.6 eV. The survey spectra were scanned in the range 0.00–1400.00 eV binding energy (BE) in 1.00 eV steps. The elemental analysis was carried out by an ICP/AES instrument (PE-SCIEX ELAN 6100 DRC).

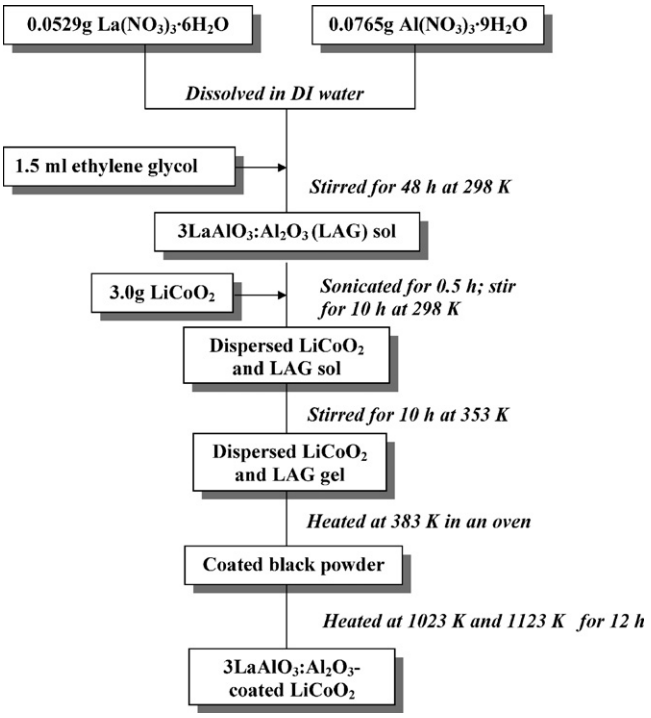

Fig. 1. Schematic for the $3LaAlO_3{:}Al_2O_3$-coated $LiCoO_2$ cathode materials prepared by an in situ sol–gel process.

The cathodes for electrochemical studies were prepared by a doctor-blade coating method. The cell performance of the cathodes was evaluated with coin-type cells of the 2032 configuration. The detailed procedure and operation were described in our previous work [11].

Coin cells cycled at different cycles were subjected to impedance measurements. The impedance spectra were recorded using a Schlumberger 1286 electrochemical interface and frequency response analyzer (Model 1255), driven by Corrware software (Scribner Associates). The frequency range was 65 kHz to 0.001 Hz and the amplitude of the perturbation signal was 20 mV. The impedance spectra were analyzed with Z-view software (Scribner Associates).

Thermal stability analysis was carried out on a PerkinElmer DSC 7 differential scanning calorimeter (DSC) for the bare and LAG-coated $LiCoO_2$ samples. The measurements were performed in a nitrogen atmosphere between 313 and 673 K, at a heating rate of 10 K min^{-1}. The samples for the DSC experiments were prepared as follows. The coin cells were first galvanostatically charged to 4.4 V at a 0.2*C* rate and then potentiostated at 4.4 V for 10 h. The coin cells were then opened inside a glove box. The cathode in the coin cell was carefully removed, and the excess electrolyte was wiped with Kimwipes. The cathode was gently scraped from the aluminum current collector, loaded on to an aluminum pan, hermetically sealed, placed in an airtight container, and transferred to the DSC instrument.

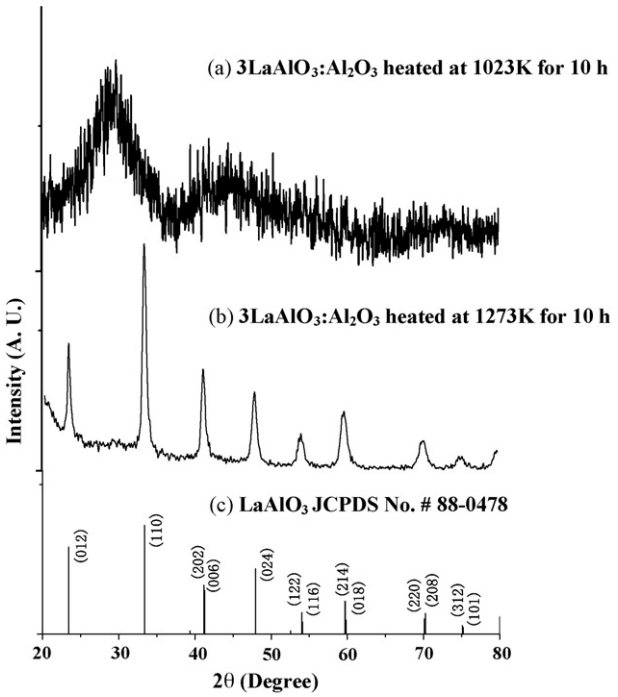

Fig. 2. X-ray diffraction patterns of the synthesized $3LaAlO_3$:Al_2O_3 particles heated for 10 h at (a) 1023 K, (b) 1273 K and (c) JCPDS data.

3. Results and discussion

3.1. X-ray diffraction

Fig. 2a–c exhibits the XRD patterns for sol–gel prepared pure $3LaAlO_3$:Al_2O_3 ceramic powders by calcination of dried gel at 1023 and 1223 K for 10 h in air, and JCPDS # 82-0478 of $LaAlO_3$, respectively. In Fig. 2a, the dried gel calcined at 1023 K remained crystalline embedded on an amorphous compound and when it was further calcined at 1223 K for 10 h in air, resulted in the complete formation of crystalline $3LaAlO_3$:Al_2O_3, in which Al_2O_3 was amorphous [23]. The pure phase of the synthesized $3LaAlO_3$:Al_2O_3 material could be indexed to the JCPDS # 82-0478 pattern [23], as shown in Fig. 2c.

Fig. 3a–d shows the XRD patterns for 1.5, 1.0 and 0.5 wt.% $3LaAlO_3$:Al_2O_3-coated $LiCoO_2$ and pristine $LiCoO_2$, respectively. The diffraction patterns of all the materials conform to a single-phase hexagonal structure of α-$NaFeO_2$ type with space group $R\bar{3}m$ symmetry of the core material. The absence of secondary phases in the complete range of diffraction patterns may correspond to the presence of low concentrations of $3LaAlO_3$:Al_2O_3 particles. The XRD patterns of the coated particles revealed that the *a* and *c* lattice parameters and the 2θ values of the peaks did not change, which indicates $3LaAlO_3$:Al_2O_3 does not form a solid solution by interacting with core material during the calcination process at 1123 K for 12 h.

3.2. Morphology

Fig. 4 shows the TEM micrographs of bare $LiCoO_2$ and LAG-coated $LiCoO_2$, as well as the micro-EDX spectrum of LAG-coated $LiCoO_2$. The TEM image in Fig. 4b displays a compact La–Al–O coating of 20–50 nm film on the surface of $LiCoO_2$ grains, which composition was confirmed by the EDX spectrum in Fig. 4c. Fig. 5 displays a scanning electron microscope (SEM) image and four corresponding EDS maps of cobalt, oxygen, alumina and lanthanum in $LiCoO_2$ coated with 1.0 wt.% $3LaAlO_3$:Al_2O_3. Very small spots were found to be highly dispersed on the coated $LiCoO_2$ particles. The spot intensity is an indicator of the element content or concentration. The denser the spot accumulation, the higher the spot content. The spots were identified as cobalt, oxygen, alumina and lanthanum by energy dispersed X-ray analysis, as shown in Fig. 5b–e, respectively. The dense accumulation of cobalt and oxygen spots in Fig. 5b and c, where these patterns were similar to coated $LiCoO_2$ particles in Fig. 5a, clearly indicated that cobalt and oxygen were from the core material of $LiCoO_2$, not from the coating material. The less dense spots of alumina and lanthanum maps in Fig. 5d and e showed a uniform distribution in the sample on the surface of the coated particles. There was no remarkable segregation of metal elements in the mapping area, which indicated that each element was uniformly coated on the surface of $LiCoO_2$ grains.

The ESCA depth profiles of the 1.0 wt.% $3LaAlO_3$:Al_2O_3-coated $LiCoO_2$ are shown in Fig. 6. It shows the O, Co, La and Al, atomic concentrations of distribution in LAG-coated $LiCoO_2$ with a depth profile of the particle. The concentration of cobalt increased down to a depth of about 10 nm and then leveled off. The high concentration of oxygen at the surface of the oxide was reasonable due to the presence of LAG oxygen content. Beyond that, there was a gradual decrease in the lanthanum and aluminum concentration with the depth of the particle. This observation indicated that a thin layer of Li–La–Al–Co–O was formed on the surface of $LiCoO_2$ that protected the $LiCoO_2$ particles from being dissolved in the electrolyte [29,30].

The surface composition of the LAG-coated $LiCoO_2$ was characterized by XPS analysis to determine whether LAG had formed a solid solution or remained on the surface of the core material. Fig. 7a–c displays the XPS spectra of O 1s, La 3d and Al 2p at depth levels of 0 and 20 nm, respectively, for the LAG-coated $LiCoO_2$ material. The O 1s spectra in Fig. 7a exhibit a median intensity peak at a

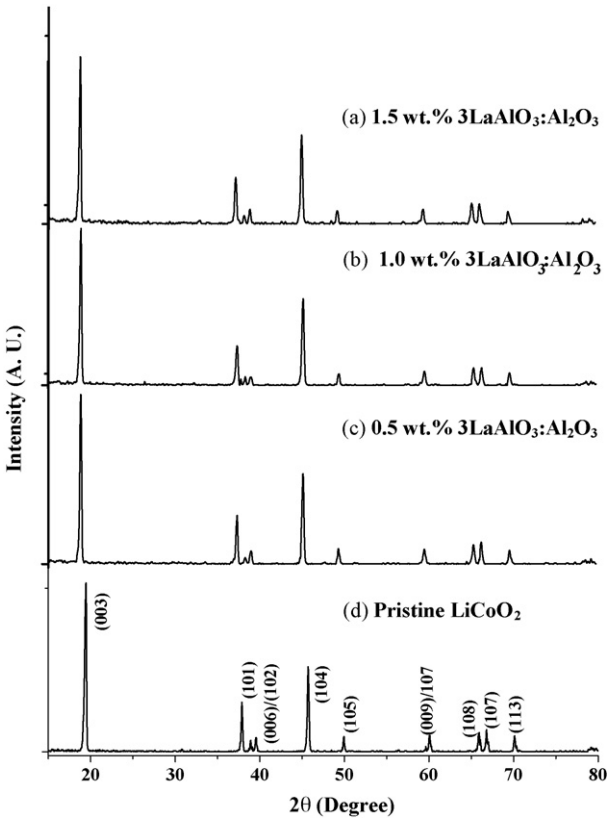

Fig. 3. X-ray diffraction patterns of (a) 1.5 wt.%, (b) 1.0 wt.%, (c) 0.5 wt.% of $3LaAlO_3$:Al_2O_3-coated $LiCoO_2$ and (d) pristine $LiCoO_2$.

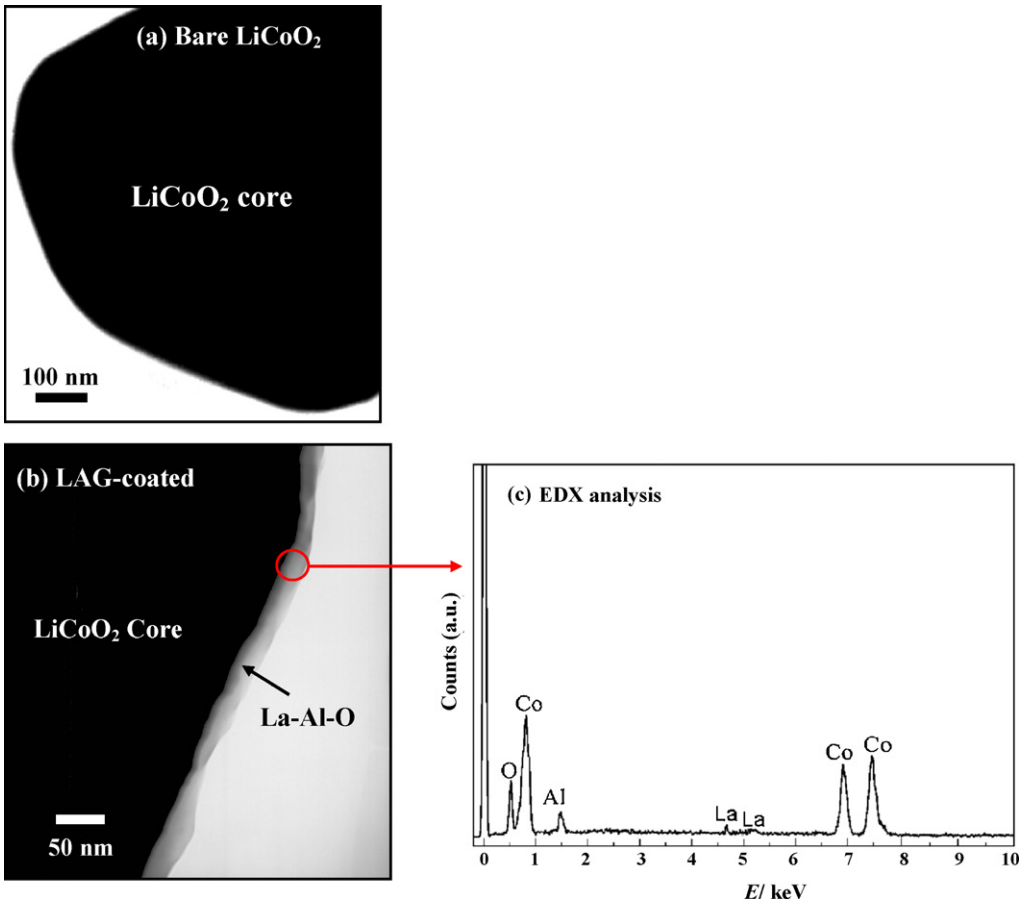

Fig. 4. TEM/EDX images of bare $LiCoO_2$ and a 1.0 wt.% $3LaAlO_3$:Al_2O_3-coated $LiCoO_2$ particle by an in situ sol–gel method.

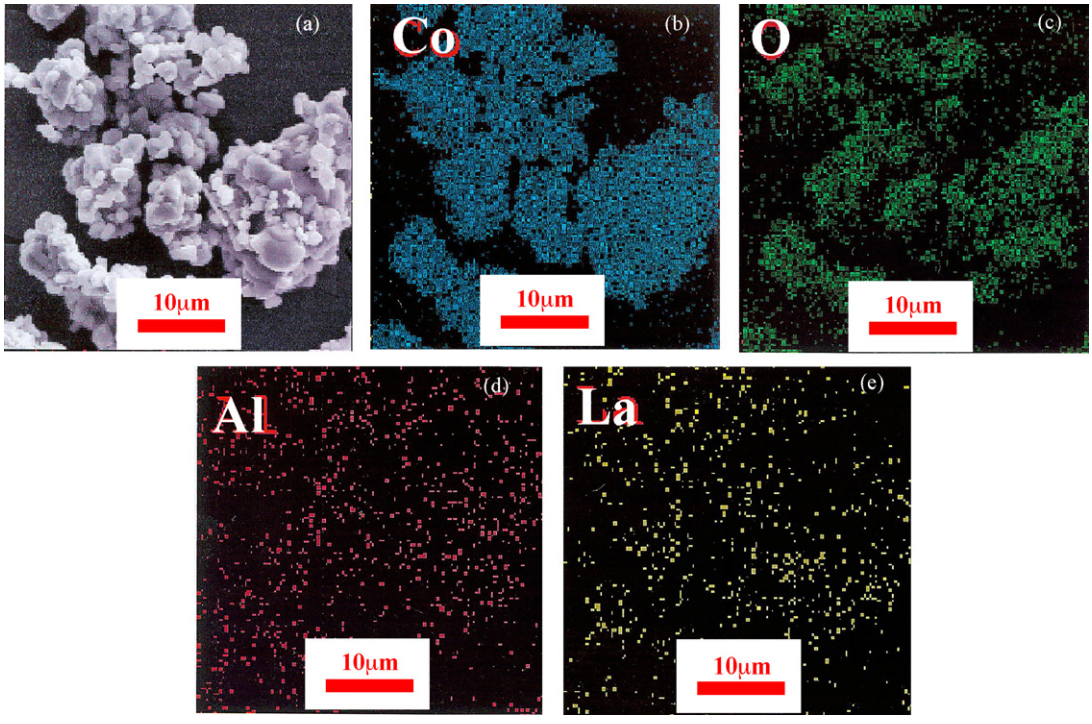

Fig. 5. A SEM image and the corresponding EDS maps of cobalt, oxygen, alumina and lanthanum in $LiCoO_2$ coated with 1.0 wt.% $3LaAlO_3$:Al_2O_3.

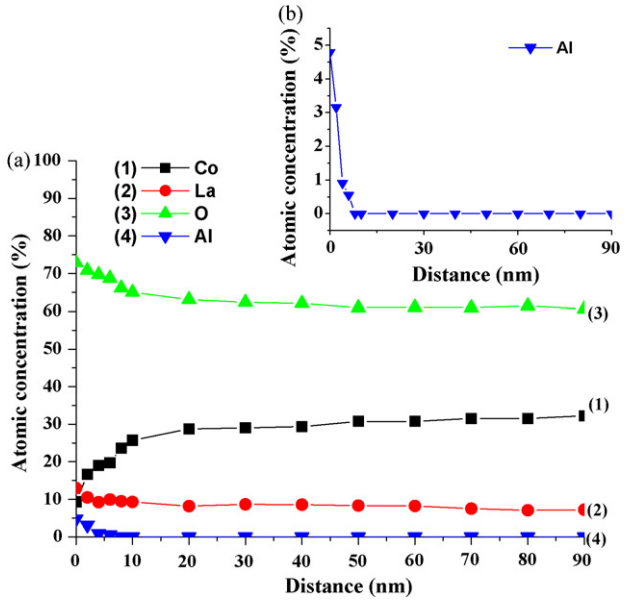

Fig. 6. (a) ESCA depth profiles of an $LiCoO_2$ particle coated with $3LaAlO_3$:Al_2O_3. (b) Depth profile of aluminum (expanded scale).

BE of 532.8 eV and a slightly higher intensity peak at a BE of 531.1 eV at a surface level of 0, which is in accordance with the reported data [31]. An intense peak at a BE of 530.5 eV refers to the oxygen ion bonded to the core material at 20 nm depth. The La 3d spectra in Fig. 7b display an intense peak centered at a BE of 834.4 eV and a broad weak band at a BE of 860.0 eV at a surface level of 0. The intense peak at 834.4 eV confirmed the presence of lanthanum originated from LAG coating on the surface of $LiCoO_2$ particles. As the depth approached 20 nm or deeper, both La 3d peaks at 860.0 and 834.4 eV shifted to 857.7 and 833.1 eV, respectively, with much weaker intensity indicating that at the surface level of zero the La ion bonded to the Al ion to form a La–Al–O thin film layer, and at the surface level of 20 nm La ion bonded to the pristine $LiCoO_2$ material. In Fig. 7c, the well-resolved peak of Al 2p at 73.62 eV was observed at a surface level of 0, but the same Al 2p peak was absent at a depth of 20 nm, indicating that Al in LAG was present at the surface of the core material as a La–Al–O thin film. Thus, it could be concluded from the different depth level analyses of O 1s, La 3d, and Al 2p that LAG not only remained on the surface as a La–Al–O thin film, but the La ion will partially diffuse into the core material to form a solid solution ($LiLa_yCo_{1-y}O_2$) during the heat treatment.

In order to demonstrate whether the La–Al–O thin film will prevent the Co oxidation to Co^{4+} or not, the amount of dissolved Co^{4+} in the electrolyte was quantitatively determined by ICP-AES analysis. As shown in Table 1, the dissolved Co content of LAG-coated $LiCoO_2$ cathodes was lower than that of pristine $LiCoO_2$. The data show that the LAG coating can effectively reduce dissociation of $LiCoO_2$ into the electrolyte and supports that LAG coating increases cyclability. Therefore, the thin film layer of La–Al–O on the surface of $LiCoO_2$ plays an important role in preserving the structure of the shell from the electrolyte.

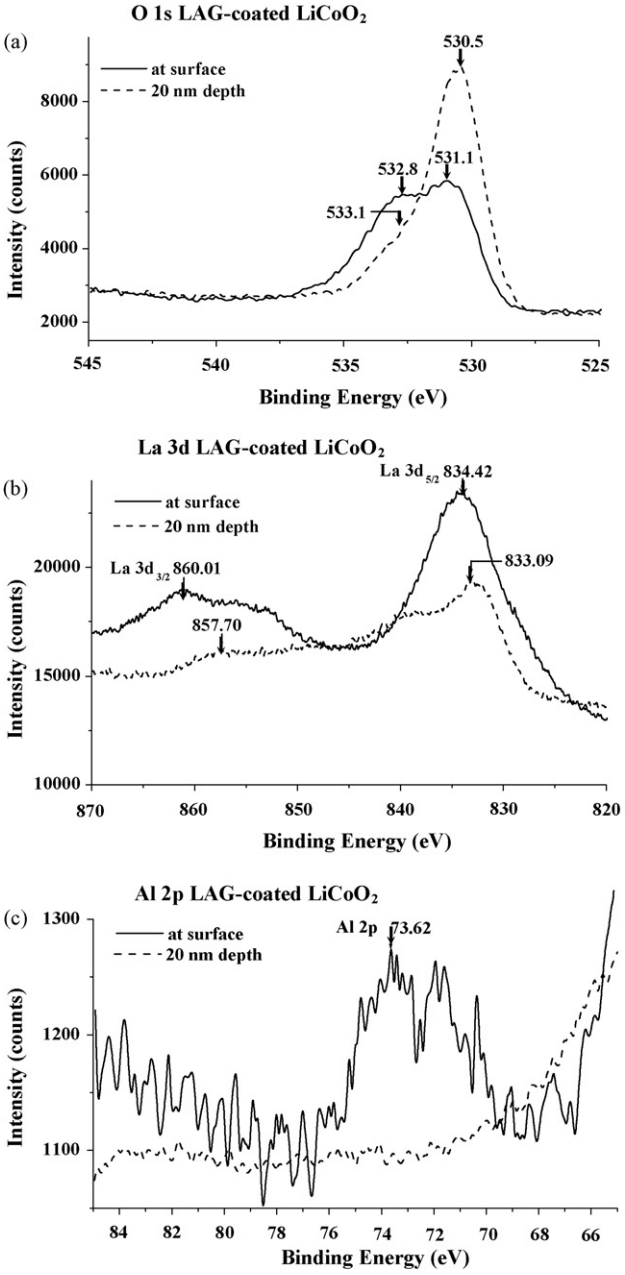

Fig. 7. XPS spectra of (a) O 1s, (b) La 3d, and (c) Al 2p of 1.0 wt.% $3LaAlO_3$:Al_2O_3-coated $LiCoO_2$ particles.

3.3. Electrochemical properties

3.3.1. Cycling performance of the coated samples calcined at different temperatures

Fig. 8 shows the discharge plots of pristine $LiCoO_2$ and 1.0 wt.% $3LaAlO_3$:Al_2O_3-coated $LiCoO_2$ samples calcined at 1023, 1123 and 1223 K between 2.75 and 4.4 V. The calcination temperature

Table 1
ICP-AES results of cobalt dissociation from $LiCoO_2$ into the electrolyte and its cyclability

wt.% of LAG-coated $LiCoO_2$	Cobalt ion concentration in electrolyte (ppm)	Initial discharge capacity (mAh g^{-1})	Cyclability (C.R. = 80%)
0.0	0.236	168	38
0.5	0.019	169	134
1.0	0.046	166	182
1.5	0.024	154	31

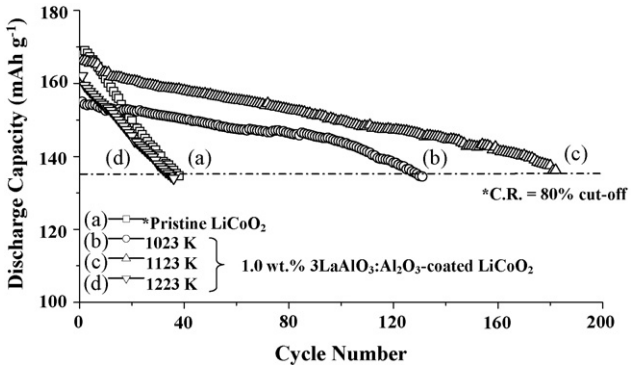

Fig. 8. Cell performance of pristine $LiCoO_2$ and 1.0 wt.% $3LaAlO_3$:Al_2O_3-coated $LiCoO_2$ heated at 1023, 1123 and 1223 K for 12 h. Charge–discharge: 4.40–2.75 V; 0.2*C* rate.

was optimized at the level where the coated samples synthesized exhibited excellent cycling performance compared to the pristine $LiCoO_2$ material. A preset cut-off value of 80% capacity retention was fixed and calculated with the first-cycle discharge capacity (value in parenthesis) for each respective material. The discharge plots in Fig. 8 show the improved cycle stability of the $3LaAlO_3$:Al_2O_3-coated samples calcined at 1023 and 1123 K compared to the pristine $LiCoO_2$ cathode material and coated sample calcined at 1223 K. Based on the cut-off regime, the pristine $LiCoO_2$ (168 mAh g^{-1}) could sustain just 38 cycles. On the other hand, the 1.0 wt.% $3LaAlO_3$:Al_2O_3-coated $LiCoO_2$ calcined at 1123 K (166 mAh g^{-1}) could sustain 182 cycles compared to 131 cycles for the samples calcined at 1023 K (155 mAh g^{-1}) and 34 cycles for the samples calcined at 1223 K (162 mAh g^{-1}). Therefore, from the discharge capacity with cycle number data, it can be concluded that the 1.0 wt.% $3LaAlO_3$:Al_2O_3-coated $LiCoO_2$ cathode material calcined at 1123 K for 12 h could yield a well-adhered coating surface on the cathode material and defend it against the electrolyte.

3.3.2. Cycling performance of the different wt.% coated samples

Fig. 9 presents the discharge plots of pristine $LiCoO_2$ and 0.5, 1.0 and 1.5 wt.% $3LaAlO_3$:Al_2O_3-coated $LiCoO_2$ cathode materials calcined at 1123 K between 2.75 and 4.4 V. The 0.5 and 1.0 wt.% $3LaAlO_3$:Al_2O_3-coated samples exhibited enhanced cycling stability compared to the 1.5 wt.% and pristine cathode materials. The number of cycles sustained by 1.0 wt.% $3LaAlO_3$:Al_2O_3-coated $LiCoO_2$ (166 mAh g^{-1}) was 182 cycles compared to 0.5 wt.% (169 mAh g^{-1}) and 1.5 wt.% (153 mAh g^{-1}) coatings that sustained 134 and 28 cycles, respectively. In general, a lower concentration of 0.5 wt.% coating would be advantageous economically,

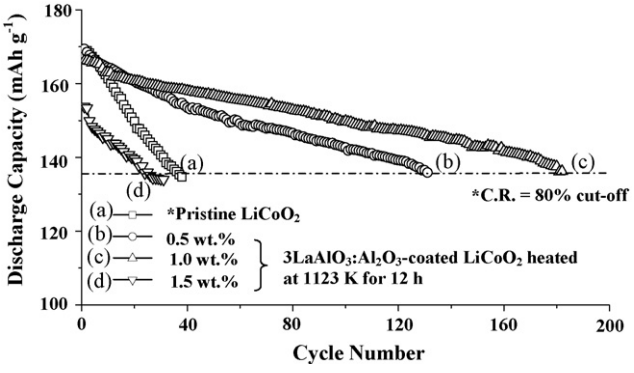

Fig. 9. Cell performance of pristine $LiCoO_2$, 0.5, 1.0 and 1.5 wt.% $3LaAlO_3$:Al_2O_3-coated $LiCoO_2$ heated at 1123 K for 12 h. Charge–discharge: 4.40–2.75 V; 0.2*C* rate.

Table 2
Comparison of the cell performance of different mixed-metal oxide coated $LiCoO_2$ electrodes

Coating materials (formula)	First-cycle capacity (mAh g^{-1})	Cyclability[a] (C.R. = 80%)	Reference
Bare $LiCoO_2$	168	38	This work
$ZrTiO_4$	166	132	[13]
$MgAl_2O_4$	164	116 (0.1*C*)	[22]
$Li_4Mn_5O_{12}$	175	125	[32]
$Y_3Al_5O_{12}$	154	165	[33]
$Li_4Ti_5O_{12}$	171	148	[34]
8 mol% Y_2O_3–92% ZrO_2	160	142	[35]
LAG ($3LaAlO_3$:Al_2O_3)	166	182	This work

[a] 4.40–2.75 V, 0.2*C* rate.

but it resulted in fewer cycles which demonstrated that the compact coating on the core material was not enough to resist faster impedance growth. On the other hand, when the coating level was increased above 1.5 wt.%, the cycle stability and initial capacity declined drastically, which could be attributed to the presence of excess coating material between the particles that lowers particle–particle electronic conductivity and adversely affects coulombic efficiency. From the charge–discharge data, it is clear that 1.0 wt.% $3LaAlO_3$:Al_2O_3 was the optimum concentration to form a compact coating buffer layer that improved cycling performance because it protected the cathode from direct interaction with the electrolyte that might have caused the formation of an organic species layer, which increased impedance and decreased capacity. It also resisted the dissolution, by a chemical interaction with the electrolyte solution, of strongly oxidized Co ions from the $Li_{1-x}CoO_2$ lattice [8,9], as shown in Table 1. The cell cycling performance of 1.0 wt.% $3LaAlO_3$:Al_2O_3-coated $LiCoO_2$ was compared to the earlier reports of mixed oxide coated $LiCoO_2$ electrodes in Table 2 [22,32–35]. It can be concluded from Table 2 that cycling performance improved after $3LaAlO_3$:Al_2O_3 was coated on the surface of the $LiCoO_2$ electrode materials.

3.3.3. Cycling performance of coated samples at different voltages

Fig. 10 exhibits the cycling performance of the coated samples cycled between 2.75 and 4.2 V, 2.75 and 4.4 V, and 2.75 and 4.6 V at a 0.2*C* rate for 25 cycles and the pristine cathode cycled at 2.75–4.4 V. In order to demonstrate the consequences of 1.0 wt.% $3LaAlO_3$:Al_2O_3 coating on cycling performance, the Li/$LiCoO_2$ cells were cycled at different charge–discharge voltages and compared to the pristine cathode material. A relatively high discharge capacity of 195 mAh g^{-1} was shown for the cell cycled at 2.75–4.6 V,

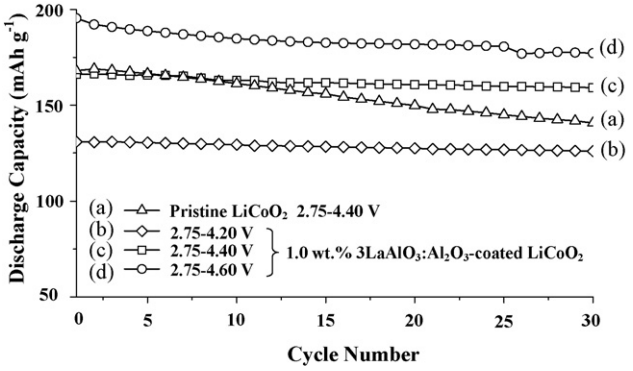

Fig. 10. Cell performance of 1.0 wt.% $3LaAlO_3$:Al_2O_3-coated $LiCoO_2$ by an in situ sol–gel method. Charge–discharge: 4.20–2.75 V; 4.40–2.75 V; 4.60–2.75 V at a 0.2*C* rate.

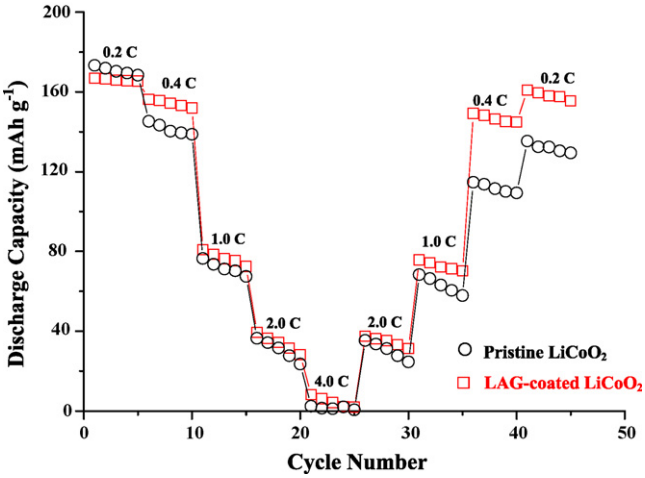

Fig. 11. Comparison of bare and 1.0 wt.% $3LaAlO_3$:Al_2O_3-coated $LiCoO_2$ by an in situ sol–gel method. Charge–discharge: 4.40–2.75 V at 0.2–4.0*C* rates.

166 mAh g^{-1} for 2.75–4.4 V and 131 mAh g^{-1} for 2.75–4.2 V. The pristine Li/$LiCoO_2$ cell cycled at 4.4 V showed a discharge capacity of 164 mAh g^{-1}, but its cycle stability declined faster compared to the coated samples even when charged or discharged at higher voltages, as in prior reports [8,9,19]. This demonstrated that the surface coating effectively protected the cathode materials by slowing impedance growth that occurred via side reactions with the electrolyte and prevented the loss of 3d metal ions so that they were readily available at higher oxidation states. The coated samples had improved discharge capacity (195 mAh g^{-1}) and cycle stability when charged at 4.6 V and these results are similar to the reports of Chen and Dahn [8,9].

3.3.4. *Cycling behavior of coated samples at different C rates*

Fig. 11 shows the rate capability data for bare and 1.0 wt.% $3LaAlO_3$:Al_2O_3-coated $LiCoO_2$ cathode materials when cycled between 2.75 and 4.4 V at different *C* rates. The discharge capacities for the coated samples at 0.2, 0.4, 1.0, 2.0 and 4.0*C* rates were 167, 156, 81, 39 and 8 mAh g^{-1}, respectively. When *C* rates were applied in the reverse order as 2.0, 1.0, 0.4 and 0.2, the cell displayed a good reversibility in discharge capacity. It indicated that the 1.0 wt.% $3LaAlO_3$:Al_2O_3-coated $LiCoO_2$ cathode material possessed significant rate capability even at higher rates and the channels for Li ion diffusion were probably not hindered by the surface buffer layer of lanthanum aluminum garnet.

3.3.5. *Impedance studies*

The impedance response of $LiCoO_2$ cathodes in non-aqueous electrolytes has contributions from processes such as the transport of lithium ions in the electrolyte, charge-transfer across the electrode–electrolyte interface, and diffusion of lithium in the solid oxide matrix [36,37]. The Nyquist plots recorded for the pristine and LAG-coated samples are presented in Fig. 12. The high-frequency semicircle represents the impedance due to a surface film on the oxide electrode, while the low-frequency semicircle is related to a slow charge transfer process at the interface, as well as a capacitance at the film/bulk oxide interface. The Warburg tail implies that the electrode processes under this condition are controlled by diffusion. The impedance spectra were analyzed by Z-view software and the data fitted to the equivalent circuit shown in Fig. 13 [38–41]. Here, R_e is the electrolyte resistance, R_p is the resistance associated with particle-to-particle contact among the oxide particles and CPE1 is the contact double-layer capacitance due to the accumulation of charged species at the surface of oxide particles. R_{ab} is

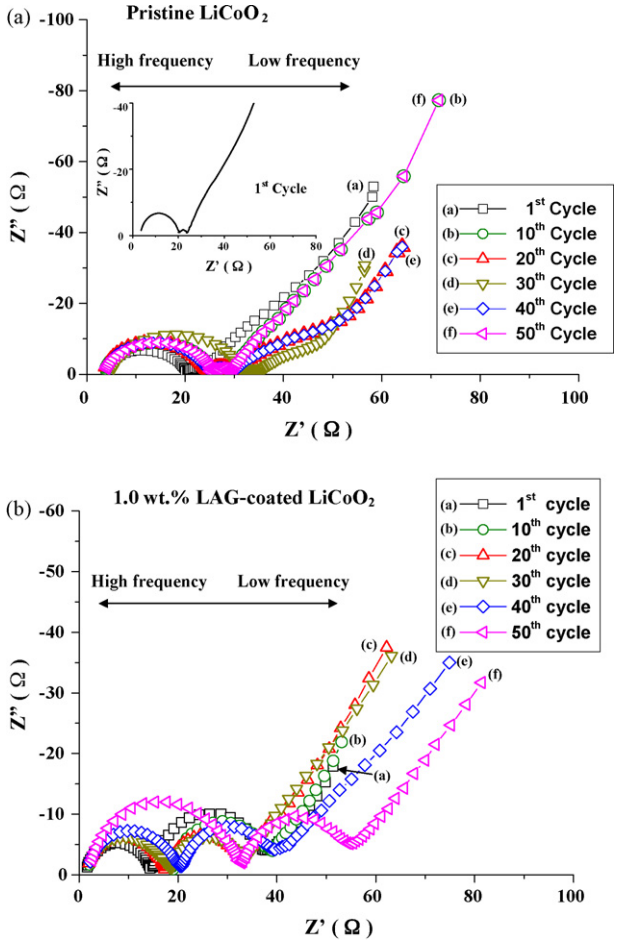

Fig. 12. Nyquist plots of (a) pristine and (b) 1.0 wt.% $3LaAlO_3$:Al_2O_3-coated $LiCoO_2$ as a function of cycle number.

the resistance associated with the absorption reaction of adsorbed lithium into the oxide and CPE2 is the capacitance arising from the adsorption of lithium in the near-surface region of the oxide. Z_W is the finite length Warburg impedance for the diffusion of lithium through the oxide film.

As can be seen from Table 3, the solution resistance, R_e, undergoes very small changes upon cycling from 2.96 to 5.94 Ω for pristine and 1.3 Ω unchanged for the coated samples. The minor changes in solution resistance are attributed to the complicated chemistry of lithium in electrolyte solutions, which leads to slight changes in the content of the conducting species in the solution [42,43]. The high-frequency resistance of the cell in Fig. 12a and b, as a function of cycle number, showed the resistance of the surface film on the cathode particles were 20.87 Ω after 10 cycles to

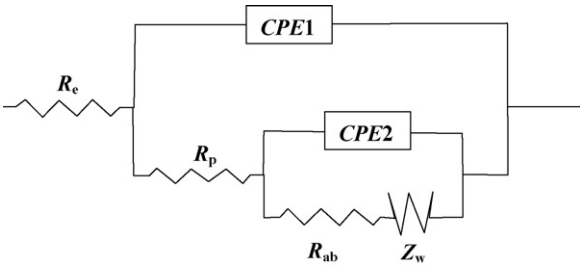

Fig. 13. Equivalent circuit used for fitting impedance data.

Table 3
Variation in the particle-to-particle resistance as a function of cycle number

Coating precursor	Cycle number	R_e (Ω)	R_p (Ω)	R_{ab} (Ω)	CPE1 (F)		CPE2 (F)		Z_W (Ω)		
					$T \times 10^{-6}$	P	$T \times 10^{-3}$	P	R	T	P
	1	2.96	17.09	3.12	7.70	0.86	7.89	0.77	56	114	0.63
	10	3.51	20.87	5.62	5.80	0.89	9.26	0.63	203	923	0.62
Pristine	20	5.39	35.67	16.28	7.60	0.90	9.63	0.64	258	1185	0.65
$LiCoO_2$	30	5.56	51.24	24.58	6.90	0.91	9.15	0.66	359	2401	0.67
	40	5.58	62.33	40.46	6.80	1.01	9.61	0.61	420	3015	0.81
	50	5.94	100.24	50.51	7.60	1.21	9.77	0.80	674	4268	0.75
	1	1.30	13.50	22.00	13.00	0.85	9.97	0.94	88	900	0.56
1.0 wt.%	10	1.30	17.50	19.00	11.30	0.83	9.97	0.94	108	1000	0.59
LAG-	20	1.30	16.50	14.00	12.10	0.83	9.97	0.91	104	1000	0.55
coated	30	1.30	17.20	14.50	12.60	0.81	9.97	0.91	103	1000	0.57
$LiCoO_2$	40	1.30	19.30	17.40	11.40	0.81	8.07	0.91	92	1000	0.48
	50	1.30	31.80	20.20	35.00	0.79	7.95	0.90	97	1000	0.53

100.24 Ω after 50 cycles for the pristine and 17.5 Ω after 10 cycles to 31 Ω after 50 cycles for the coated sample (Table 3). Therefore, the pristine sample showed an increase in resistance of 79.37 Ω for 40 cycles, while the coated sample showed an increase of 13.5 Ω for 40 cycles. Table 3 also shows the resistance associated with the absorption reaction, R_{ab}, of the cathode materials increased as the cycling proceeded for pristine compared to coated samples. This result corresponds to a fast increase in impedance growth over the surface by a passive film on the pristine vs. the LAG-coated $LiCoO_2$. Thus, the equivalent circuit model remains the best fit of the Nyquist plot measured for both pristine $LiCoO_2$ and coated $LiCoO_2$. In the case of pristine and coated $LiCoO_2$, the angle of depression of the second semicircle varied depending on the insulation layer on the surface of the $LiCoO_2$.

The impedance results revealed that the passive surface film [42,43], which formed on the pristine cathode particles increased resistance faster with cycle number (Fig. 12a). In contrast, formation of the passive surface film was controlled and the reaction between the electrolyte and the oxide particles was suppressed on the LAG-coated $LiCoO_2$ surface (Fig. 12b). The constituents of the surface passive film (polycarbonates, polymeric hydrocarbons, Li_2CO_3, LiF, Li_xPF_y and $Li_xPF_yO_z$) formed on the cathode particles during the electrochemical reaction changes with the oxide and the electrolyte that increases the resistance of the surface film and dynamically hinders the movement of the lithium ion during the (de)lithiation process [38,39]. Thus, during cycling, the formation of a passive surface film, resulting in impedance growth of the pristine $LiCoO_2$ resulted in faster capacity fade and lower cycle stability during repeated cycling compared to LAG-coated $LiCoO_2$ samples.

3.4. Thermal stability studies

One key requirement for the use of battery-active materials in commercial products is their thermal stability because of safety concerns. $Li_{0.5}CoO_2$ is known to decompose at temperatures above 473 K [44] through loss of oxygen according to the equation [45]:

$$Li_{0.5}CoO_2 \rightarrow (1/2)LiCoO_2 + (1/6)Co_3O_4 + (1/6)O_2$$

Fig. 14 shows the DSC curves for overcharged pristine $LiCoO_2$ and LAG-coated $LiCoO_2$. It can be seen from Fig. 14a that the maximum on the heat profile occurs at 453 K for the pristine $LiCoO_2$. However, maximum heat flow was observed at 458 K for the LAG-coated sample (Fig. 14b). Thus, the coating renders the cathode material less reactive towards the electrolyte, enhancing its thermal stability. The higher decomposition temperature of the coated material was complemented by its lower enthalpy of reaction (163 J g^{-1}) compared to the bare oxide (187 J g^{-1}), as in shown Table 4. It is known that an exothermic reaction depends on the concentration of reactants such as delithiated Li_xCoO_2 and the amount of electrolyte compounds [46–48].

Fey et al. [49] reported that the poor structure stability of Li_xCoO_2, when cycled to high voltages above 4.2 V, could be improved by coating cobalt oxide on the surface of $LiCoO_2$. In addition, they [12] also reported that the exothermic peak corresponding to the release of oxygen at ~464 K was significantly smaller for the La_2O_3-coated cathode material, reflecting its high thermal stability. Cho et al. suggested that the $AlPO_4$ [50–52], Al_2O_3 [51] and P_2O_5 [52] coatings might inhibit side reactions, which result in oxygen loss from Li_xCoO_2 to the electrolyte, and thereby improve the cycling stability. The total heat evolution decreased from 320 W g^{-1} for bare $LiCoO_2$ to 0.1 W g^{-1} for $AlPO_4$-coated $LiCoO_2$ samples [50]. However, the onset temperatures of the $AlPO_4$-coated $LiCoO_2$ increased to 490 K, from 460 K for the bare samples. Cho et al. [52] also pointed out that the results of both the P_2O_5-coated and $AlPO_4$-coated samples showed that the initial exothermic-reaction temperatures with flammable electrolytes increased to 503 K (453 K for bare $LiCoO_2$), and the coatings greatly reduced the amount of exothermic heat generated by approximately one order of magnitude compared to bare $LiCoO_2$. Omanda et al. [53] reduced the exothermic reaction ~50% with SiO_2-coated $LiNi_{0.8}Co_{0.2}O_2$ after charging the cells to 4.3 V. Table 4 presents a comparison of the thermal analysis data for LAG-coated $LiCoO_2$ with previously reported results for coated $LiCoO_2$ and $LiNi_{0.8}Co_{0.2}O_2$ electrode materials.

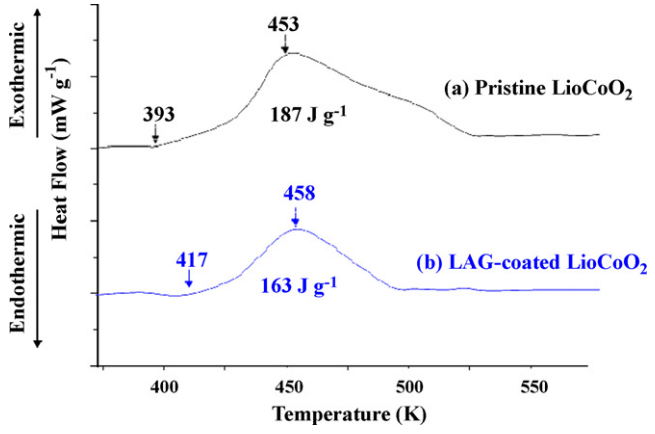

Fig. 14. DSC scans of (a) pristine and (b) 1.0 wt.% $3LaAlO_3$:Al_2O_3-coated $LiCoO_2$ after five cycles with full charge at 4.4 V vs. Li for 10 h.

Table 4
Comparison of the DSC results for pristine and LAG-coated $LiCoO_2$ samples

Authors	Samples	Decomposition temperature (K)	Exothermic enthalpy ($J\,g^{-1}$)	Condition	Reference
Fey et al.	Pristine Li_xCoO_2	453	187	After five cycles with full charge at 4.4 V for 10 h at 0.2*C* rate	This work
	1.0 wt.% LAG-coated Li_xCoO_2	458	163		
	Pristine Li_xCoO_2	525	12.8	Charged to 4.4 V at 0.1C rate	[49]
	0.3 wt.% cobalt oxide-coated Li_xCoO_2	536	8.8		
	Pristine Li_xCoO_2	458	The relative exothermic area under the peak was smaller by a factor of 3 times vs. the pristine material	Charged to 4.6 V at 0.2*C* rate	[12]
	2.0 wt.% La_2O_3-coated Li_xCoO_2	464			
Cho et al.	Pristine Li_xCoO_2	373	320	Charged to 4.7 V at 0.1C rate	[50]
	P10-$AlPO_4$-coated Li_xCoO_2	490	35		
	Pristine Li_xCoO_2	443	–	Charged to 4.3 V	[51]
	Al_2O_3-coated Li_xCoO_2	463	–		
	$AlPO_4$-coated Li_xCoO_2	503	–		
	Pristine Li_xCoO_2	453	–	Charged to 4.3 V	[52]
	P_2O_5-coated Li_xCoO_2	503	–		
Omanda et al.	Pristine $Li_xNi_{0.8}Co_{0.2}O_2$	487	462	Charged to 4.3 V at C/16 rate	[53]
	SiO_2-coated $Li_xNi_{0.8}Co_{0.2}O_2$	476	207		

4. Conclusions

Different wt.% $3LaAlO_3$:Al_2O_3-coated $LiCoO_2$ cathode materials were successfully prepared by an in situ sol–gel process. The XRD patterns confirmed that the core material retained its original structure without any alteration upon coating with different wt.% of $3LaAlO_3$:Al_2O_3 particles. The TEM image displayed that $3LaAlO_3$:Al_2O_3 was formed as a compact layer over the $LiCoO_2$ cathode particle. Coating improved cycle stability by primarily protecting the cathode surface from thick impedance film formation that is normally attributed to the surface chemistry of $LiCoO_2$ and the reactivity of the electrolyte at higher voltage charge–discharge processes. The 1.0 wt.% $3LaAlO_3$:Al_2O_3-coated $LiCoO_2$ cathode displayed excellent cycle stability of 182 cycles, which was superior to 38 cycles sustained by the pristine $LiCoO_2$ cathode material when cycled between 2.75 and 4.4 V.

Acknowledgements

Financial support for this work was provided by the National Science Council of the Republic of China under contract No. NSC 93-2214-E-008-004. PMD thanks the NSC for the award of a postdoctoral fellowship.

References

[1] L.D. Dyer, B.S. Borie Jr., G.P. Smith, J. Am. Chem. Soc. 76 (1954) 1499.
[2] H.F. Wang, Y.I. Jang, B.Y. Huang, D.R. Sadoway, Y.M. Chiang, J. Electrochem. Soc. 146 (1999) 473.
[3] G.G. Amatucci, J.M. Tarascon, L.C. Klein, Solid State Ionics 83 (1996) 167.
[4] J.M. Tarascon, M. Armand, Nature (London) 414 (2001) 359.
[5] C. Julien, S. Gastro-Garcia, J. Power Sources 97–98 (2001) 290.
[6] M. Winter, J.O. Besenhard, M.E. Spahr, P. Novák, Adv. Mater. 10 (1998) 725.
[7] J. Cho, G. Kim, Electrochem. Solid-State Lett. 2 (1999) 253.
[8] Z. Chen, J.R. Dahn, Electrochem. Solid-State Lett. 5 (2002) A213.
[9] Z. Chen, J.R. Dahn, Electrochim. Acta 49 (2004) 1079.
[10] N.V. Kosova, E.T. Devyatkina, J. Power Sources 174 (2007) 959.
[11] G.T.K. Fey, C.-F. Huang, P. Muralidharan, E.S.S. Chang, J. Power Sources 174 (2007) 1147.
[12] G.T.K. Fey, P. Muralidharan, C.Z. Lu, Y.D. Cho, Electrochim. Acta 51 (2006) 4850.
[13] G.T.K. Fey, C.Z. Lu, J.D. Huang, T.P. Kumar, Y.C. Chang, J. Power Sources 146 (2005) 65.
[14] A.M. Kannan, L. Rabenberg, A. Manthiram, Electrochem. Solid-State Lett. 6 (2003) A16.
[15] G.T.K. Fey, H.M. Kao, P. Muralidharan, T.P. Kumar, Y.D. Cho, J. Power Sources 163 (2006) 135.
[16] G.T.K. Fey, J.G. Chen, T.P. Kumar, J. Appl. Electrochem. 35 (2005) 177.
[17] K.Y. Chung, W.S. Yoon, J. McBreen, X.Q. Yang, S.H. Oh, H.C. Shin, W.I. Cho, B.W. Cho, J. Power Sources 174 (2007) 619.
[18] H.W. Ha, N.J. Yun, M.H. Kim, M.H. Woo, K. Kim, Electrochim. Acta 51 (2006) 3297.
[19] J. Cho, T.G. Kim, C. Kim, J.G. Lee, Y.W. Kim, B. Park, J. Power Sources 146 (2005) 58.
[20] J.G. Lee, T.G. Kim, B. Park, Mater. Res. Bull. 42 (2007) 1201.
[21] H. Wang, W.D. Zhang, L.Y. Zhu, M.C. Chen, Solid State Ionics 178 (2007) 131.
[22] G.T.K. Fey, Z.F. Wang, C.Z. Lu, T.P. Kumar, J. Power Sources 146 (2005) 245.
[23] A. Leleckaite, A. Kareiva, Opt. Mater. 26 (2004) 123.
[24] R.C. Pullar, M.D. Taylor, A.K. Bhattacharya, J. Eur. Ceram. Soc. 19 (1999) 1747.
[25] M. Veith, S. Mathur, A. Kareiva, M. Jilavi, M. Zimmer, V. Huch, J. Mater. Chem. 9 (1999) 3069.
[26] K. Xiong, J. Robertson, S.J. Clark, Microelectron. Eng. 85 (2008) 65.
[27] L. John Berchmans, S. Angappana, A. Visuvasama, K.B. Ranjith Kumar, Mater. Chem. Phys. 109 (2008) 113.
[28] M. Nieminen, T. Sajavaara, E. Rauhala, M. Putkonen, L. Niinistö, J. Mater. Chem. 11 (2001) 2340.
[29] N. Van Landschoot, E.M. Kelder, P.J. Kooyman, C. Kwakernaak, J. Schoonmana, J. Power Sources 138 (2004) 262.
[30] A.T. Appapillai, A.N. Mansour, J. Cho, Y.S. Horn, Chem. Mater. 19 (2007) 5748.
[31] http://www.xpsdata.com/XI_BE_Lookup_table.pdf.
[32] C.F. Huang, Master thesis, National Central University, Taiwan, ROC, 2006. http://thesis.lib.ncu.edu.tw/ETD-db/ETD-search-c/view_etd?URN=93324032.
[33] J.M. Chen, C.L. Hsiao, G.T.K. Fey, Abstracts of the 2007 Conference of the International Battery Materials Association, Shenzhen, China, 2007, p. 115.
[34] G.T.K. Fey, C.F. Huang, P. Muralidharan, E. Chang, J. Power Sources 174 (2007) 1147.
[35] G.T.K. Fey, C.L. Hsiao, P. Muralidharan, J. Nanomaterials, in press.

[36] D. Aurbach, M.D. Levi, E. Levi, H. Teller, B. Markovsky, G. Salitra, L. Heider, U. Heider, J. Electrochem. Soc. 145 (1998) 3024.
[37] F. Croce, F. Nobili, A. Deptula, W. Lada, R. Tossici, A. D'Epifanio, B. Scrosati, R. Marassi, Electrochem. Commun. 1 (1999) 605.
[38] M.G.S.R. Thomas, P.G. Bruce, J.B. Goodenough, J. Electrochem. Soc. 132 (1985) 1521.
[39] K. Xu, Chem. Rev. 104 (2004) 4303.
[40] Y.M. Choi, S.I. Pyun, S.I. Moon, Solid Stale Ionics 89 (1996) 43.
[41] H.E. Conway, J. Electrochem. Soc. 138 (1991) 1569.
[42] D. Aurbach, A. Schechter, Electrochim. Acta 46 (2001) 2395.
[43] D. Aurbach, B. Markovsky, M.D. Levi, E. Levi, A. Schechter, M. Moshkovich, Y.S. Cohen, J. Power Sources 81–82 (1999) 95.
[44] J. Cho, Y.J. Kim, T.J. Kim, B. Park, Chem. Mater. 13 (2001) 18.
[45] H.J. Kweon, S.J. Kim, D.G. Park, J. Power Sources 88 (2000) 255.
[46] H. Maleki, G. Deng, A. Anani, J. Howard, J. Electrochem. Soc. 146 (1999) 3224.
[47] Y. Baba, S. Okada, J. Yamaki, Solid State Ionics 148 (2000) 311.
[48] D.D. Macneil, J.R. Dahn, J. Electrochem. Soc. 148 (2001) A1205.
[49] G.T.K. Fey, Y.Y. Lin, T.P. Kumar, Surf. Coat. Technol. 191 (2005) 68.
[50] J. Cho, Electrochim. Acta 48 (2003) 2807.
[51] J. Cho, T.G. Kim, C. Kim, J.G. Lee, Y.-W. Kim, B. Park, J. Power Sources 146 (2005) 58.
[52] J. Cho, J.G. Lee, B. Kim, B. Park, Chem. Mater. 15 (2003) 3190.
[53] H. Omanda, T. Brousse, C. Marhic, D.M. Schleich, J. Electrochem. Soc. 151 (6) (2004) A922.